Mesoscale Instability and Upwelling. Part 2: Testing the Diagnostics of Vertical Motion with a Three-Dimensional Ocean Front Model*

VOLKER H. STRASS

Alfred-Wegener-Institut für Polar- und Meeresforschung, Bremerhaven, Germany

(Manuscript received 25 August 1992, in final form 1 November 1993)

ABSTRACT

A three-dimensional primitive equation ocean front model is employed to simulate mesoscale instabilities and then to investigate the validity (and the contingent differences) of three alternative methods used for the diagnosis of mesoscale vertical motion from combined density and horizontal velocity mappings: 1) the isopycnic advection equation, 2) the vorticity advection equation, and 3) the ω equation. The model is integrated for 60 days during which period meanders form along the initially unidirectional jet, first preferably at a wavelength of just under 100 km and later also at smaller horizontal scales; these growing instabilities are associated with vertical velocities of up to some tens of meters per day. The horizontal distribution pattern of vertical velocity can reasonably be estimated by use of method 3 and also method 2, but method 1 may yield a pattern having the wrong phase relationship.

1. Introduction

Knowledge of the mesoscale distribution of vertical velocity in the ocean is of central importance to gaining insight to the dynamical behavior of the flow, because a distinct pattern of vertical motion is associated with meanders and eddies that form due to baroclinic instability (e.g., Gill 1982, chapter 13; Pedlosky 1987, chapter 7). It also matters in the realm of biological oceanography because nutrient pulses caused by mesoscale upwelling events stimulate the primary production and thus significantly modify the horizontal distribution of phytoplankton chlorophyll (Woods 1988; Strass 1992).

However, synoptic maps of vertical velocity cannot yet be obtained from direct measurements. As a way out, methods of diagnosing the mesoscale distribution of vertical motion from combined density and horizontal velocity mappings have been proposed (Leach 1987; Tintoré et al. 1991; Fiekas et al. 1994). These methods are based on application of either 1) the isopycnic advection equation, 2) the vorticity advection equation, or 3) the Q-vector version of the ω equation developed by Hoskins et al. (1978). Whereas methods 1 and 2 each represent only one of the two effects contributing to the forcing of vertical motion, the divergence of Q vectors in method 3 comprises the total forcing, albeit only to the accuracy of quasigeostrophy (Hoskins et al. 1978; Hoskins and Pedder 1980). Of course, for flows with higher Rossby number only the primitive equations will suffice to describe the motion field. Consequently, the data analyses reported in earlier publications and in the companion paper by Fiekas et al. (1994) have revealed differences of the three diagnostic methods, without being able to provide conclusive means of discriminating between their diagnostic qualities.

In this study the three methods of diagnosing mesoscale vertical motion are tested. The test is carried out with the aid of a three-dimensional ocean front model based on the primitive equations.

The model-calculated vertical velocity pattern must not necessarily resemble nature exactly, but it is internally consistent with the other fields of model variables like density and horizontal velocity. Compared to the patterns of vertical motion diagnosed by methods 1–3, obtained by neglecting various terms in the governing equations and making simplifying assumptions, the vertical velocity field calculated from the model equations may be considered as being closest to nature. While the model run is not intended to be a direct simulation of the observed situation reported in the companion paper it nevertheless contains situations that can be related to the ones observed.

2. Materials and methods

The model employed is the quasi-isopycnic ocean circulation model introduced by Bleck and Boudra (1981). It is based on the primitive equations in an *f*-

* Alfred-Wegener-Institut für Polar- und Meeresforschung Contribution Number 574.

Corresponding author address: Dr. Volker H. Strass, Alfred-Wegener-Institut für Polar- and Meeresforschung, Postfach 120161, Columbusstrasse, D-7515 Bremerhaven, Germany.

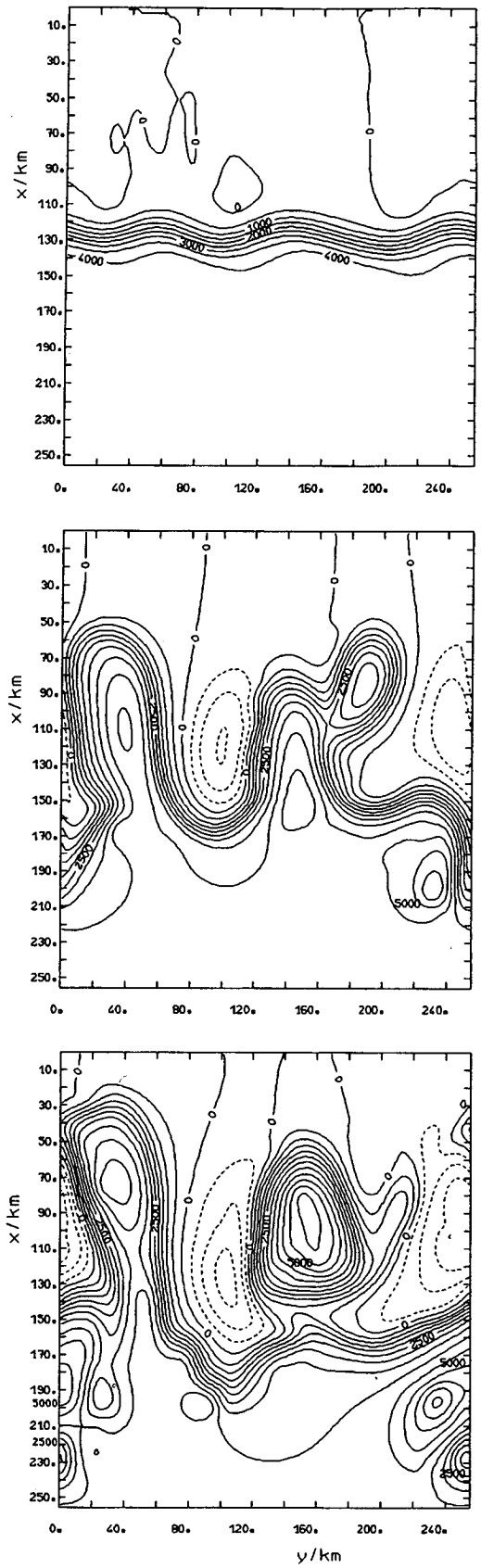

plane approximation, the adiabatic thermodynamic equation, the hydrostatic equation, and the continuity equation from which the vertical velocity is calculated. The advantage of this model formulation using quasi-isopycnic coordinates is that potential vorticity is conserved (Bleck 1979). The model is meanwhile well established (e.g., Boudra et al. 1988; Bleck et al. 1989; Bleck and Smith 1990; Onken and Klein 1991; Onken 1992), and the version used in this study is almost identical to that thoroughly described by Onken (1986, 1992). Hence, only some special features and parameter settings will be reported here.

The domain of the model is a channel-type rectangular box made up of vertical walls, a flat bottom at a pressure level of $p = 1000$ dbar, and a rigid-lid surface damping out gravity waves. Because of the f-plane approximation the orientation of the box in the geographic coordinate frame does not matter, but for convenience and comparison with the field measurements the x direction is regarded running from north to south and y from west to east. At the zonal solid walls free-slip boundary conditions are applied, and periodic boundary conditions at the open meridional walls. The horizontal plane of the model is made up of a 256 km $\times$ 256 km square, divided in 128 $\times$ 128 grid points, respectively, resolved for x and y by 2-km intervals. In the vertical the box is partitioned by 6 levels into 5 layers. The model integration is initiated with a unidirectional zonal jet in geostrophic balance, which then is superimposed by an ageostrophic barotropic random (white noise) perturbation field of small amplitude (for details see Onken 1992).

The initial density distribution in the top layers is adjusted to that found in the seasonal thermocline during a survey at the North Atlantic Polar Front, which provides the field database for the analysis contained in the companion paper by Fiekas et al. (1994). The density layer analyzed in the model (layer 2) initially slopes down from north to south from 12- to 71-m depth over the meridional model extent (256 km); the isopycnic surface used for the data analysis (covering 1°50′ of latitude, approximately 204 km) varies between 22 and 57 m. The Coriolis parameter is set to 115 rad Ms^{-1}, corresponding to 52°N, which is the central latitude of the North Atlantic Polar Front survey.

The meridional variation of the planetary vorticity is neglected by the model (f-plane approximation). This seems justified by the confined north–south model ex-

FIG. 1. Modeled streamfunction (in units of m^2 s^{-1}) at integration day 20 (top), 50 (middle), and 60 (bottom) of layer 2 at an average depth of 49 m. The increment of the streamfunction contours is 500 m^2 s^{-1}. The absolute minima and maxima have values of -108 and 4352 m^2 s^{-1} at day 20, -1527 and 5933 m^2 s^{-1} at day 50, and -1985 and 6595 m^2 s^{-1} at day 60. The direction of flow in the initial jet is from left to right.

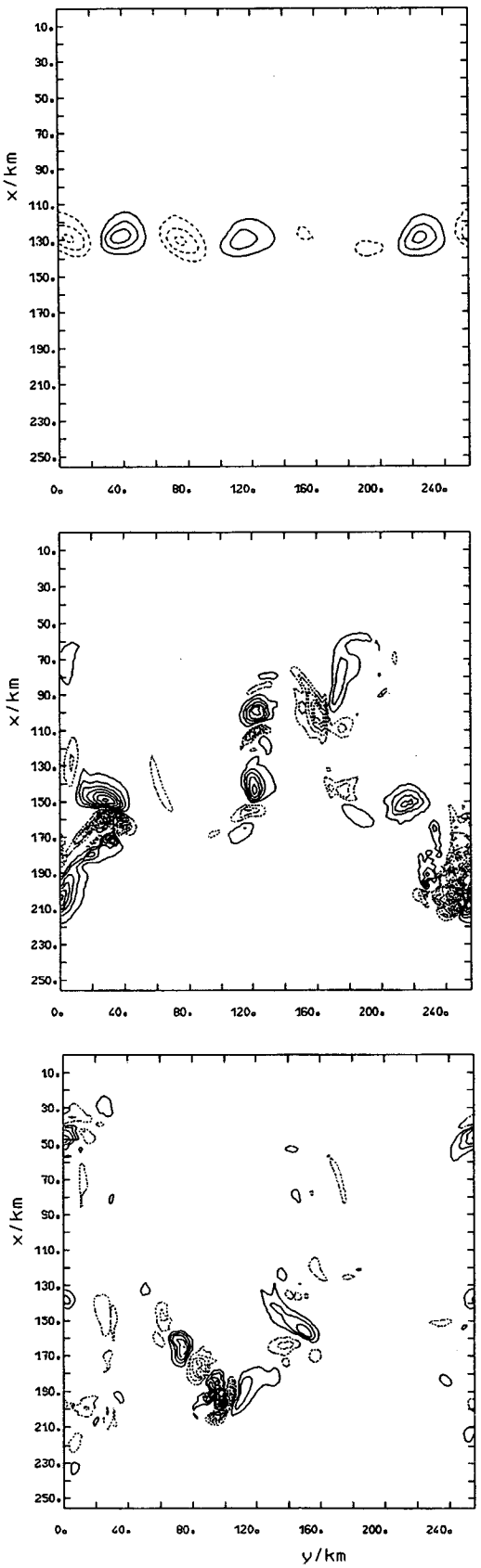

tent. One result of the data analysis presented in the companion paper by Fiekas et al. (1994) is that the contribution by the β term to the forcing of mesoscale vertical motion is indeed negligible compared to the other terms.

The model was integrated for 60 days. Then integration was stopped because the horizontal current field had spread from the interior of the model domain to the northern and southern boundaries, and it was expected that during further integration the model results would be influenced more strongly by the channel-like nature of the model box and no longer resemble unbounded open ocean flows in which we were most interested.

To test the methods of diagnosing mesoscale vertical motion by use of either 1) the isopycnic advection equation, 2) the vorticity advection equation, or 3) Q vectors, these three methods are applied to the modeled density and horizontal velocity fields in exactly the same manner as to field data as described in the companion paper by Fiekas et al.; this involves, for instance, fitting a streamfunction to the modeled horizontal velocities before application of the diagnostics. The horizontal grid, however, is that given by the model resolution of 2 km. Method 1 is based on Eq. (8) in the companion paper, a simplified form of the adiabatic thermodynamic equation. Method 2 uses Eq. (4) but neglects the β term, $v\beta$, in calculating the divergence implied by the advection of relative vorticity. Method 3 is based on Eqs. (11) and (12) in the companion paper, with Eq. (11) defining the Q vectors and Eq. (12) being the Q-vector version of the ω equation; the divergence of the Q-vector field, however, is calculated without taking into account the negligible β term in Eq. (12). The ω equation is generally taken to be a wave equation so that the vertical velocity is related to the convergence of Q vectors (Hoskins et al. 1978); convergence of the Q vectors means upwelling, that is, positive vertical velocity, and divergence means downwelling. In the analysis of the data (Leach 1987; Fiekas et al.), a potential χ is calculated from the divergence of Q vectors, which retains the form of the Q-vector divergence but is smoother.

The different horizontal distribution patterns of vertical motion implied by methods 1–3 are each compared to the modeled vertical velocity field. For objective comparison and in order to obtain an overall statistical mean estimate of the diagnostic accuracy of each

FIG. 2. Modeled horizontal distribution pattern of the vertical motion (in units of m d^{-1}) at integration day 20 (top), 50 (middle), and 60 (bottom) at level 2 with an average depth of 41.5 m. The contour increment is 1 m d^{-1} at day 20, 2.5 m d^{-1} at day 50, and 5 m d^{-1} at day 60; the contour of zero vertical velocity is not drawn. The absolute minima and maxima of vertical velocity have values of −3.3 and 3.6 m d^{-1} at day 20, −29.4 and 18.3 m d^{-1} at day 50, and −72.9 and 40.7 m d^{-1} at day 60; positive means upwelling.

TABLE 1. Minima and maxima of the modeled vertical velocity (w), the diagnosed divergence implied by vorticity advection (DV), the convergence of Q vectors ($-$DQ), and the Q-vector potential (χ).

Day	w [m d^{-1}]	DV [d^{-1}]	$-$DQ [m^{-1} d^{-1}]	$-\chi$ [m d^{-1}]
20	−3.3, 3.6	−0.087, 0.085	−0.158, 0.148	−6.9, 8.6
30	−7.9, 8.3	−0.184, 0.264	−0.480, 0.414	−22.5, 17.3
40	−10.7, 10.0	−0.263, 0.268	−0.562, 0.396	−38.0, 18.1
50	−29.4, 18.3	−1.146, 0.703	−1.801, 1.256	−44.9, 24.2
60	−72.9, 40.7	−1.008, 1.194	−1.419, 1.341	−64.8, 48.4

method, the coherence and phase spectra of the three implied and the modeled fields of vertical velocity are calculated. For spectral analysis, the horizontal (or isopycnic in effect) data fields are divided into 128 rows of 128 data points each, with the rows aligned along the y direction (the direction of the initial jet); the Fourier coefficients calculated from each of the 128 rows are then averaged to obtain one spectrum for the complete layer. Estimation of the confidence level of coherence, however, takes into account that not all the 128 rows are statistically independent.

3. Results

During the first 20 days of the model run, a quasi-sinusoidal meander structure develops along the initially unidirectional jet, which is considered as flowing zonally from west to east (Fig. 1 top). The meander structure has zonal wavenumber $\kappa = 3$, that is, a wavelength of about 85 km given by the model extent of 256 km. As integration continues, the meander amplitude grows generally. Especially fast growing is the third (viewed from the left-hand side) ridge, a northward extension of the streamlines with anticyclonic curvature. This ridge is the first to start shedding an eddy. However, before this eddy has completely separated, it interacts and recombines around day 50 with the second ridge, which also is growing (Fig. 1 middle). After this interaction of the second and third ridge, an anticyclonic eddy of about 100 km diameter, located in the upper-right (northeast) quarter of the model domain has formed by day 60 (Fig. 1 bottom); the remaining meander structure, composed of a narrow ridge on the left side and a broad trough on the right side of the model domain, has the basic wavenumber $\kappa = 1$, that is, a wavelength of 256 km. The streamline

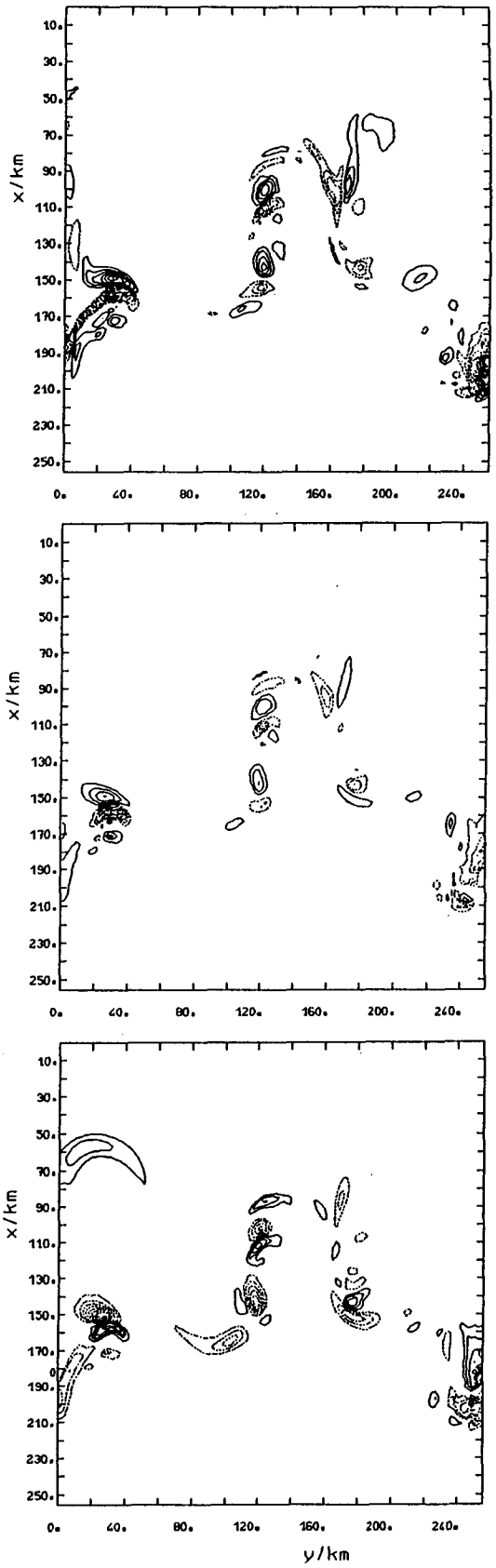

FIG. 3. Horizontal distribution pattern of vertical motion implied by the convergence of Q vectors (top), by the divergence resulting from advection of vorticity (middle), and by isopycnic advection (bottom), on the basis of model data at day 50. The contour increment is 2 Ms^{-1} m^{-1} for the convergence of Q vectors (top), 2 Ms^{-1} for the divergence resulting from vorticity advection (middle), and 0.05 mm s^{-1} for the vertical velocity implied by isopycnic advection (bottom); zero contours are not shown.

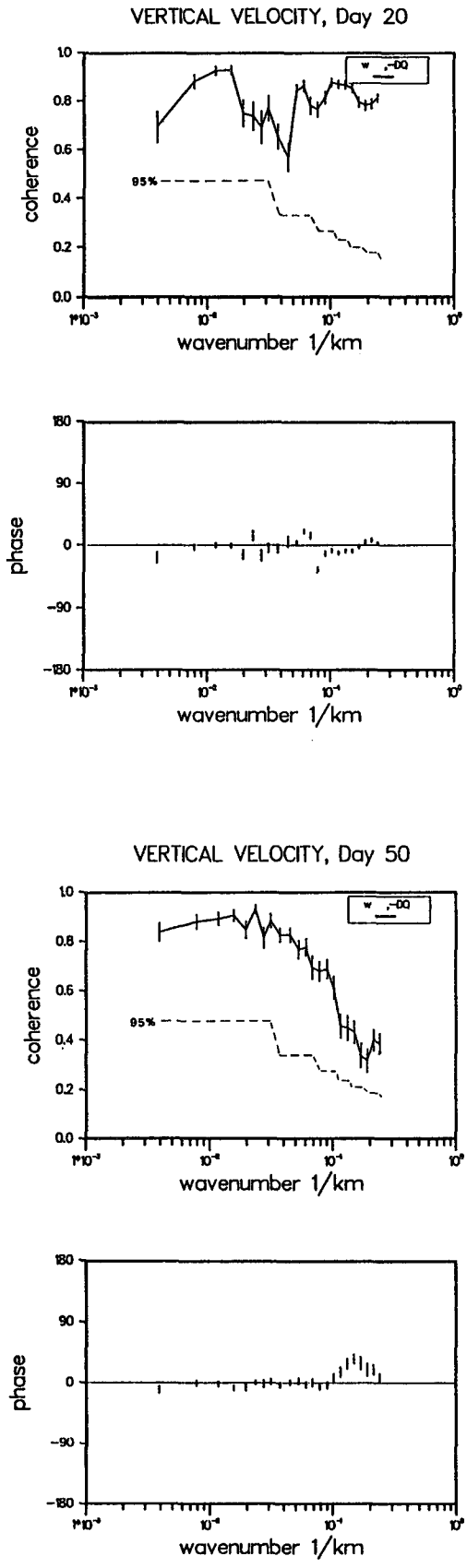

pattern appearing in the model domain at day 60 shows similarities to that found during the survey of the North Atlantic Polar Front (see Fig. 5 in the companion paper by Fiekas et al., this volume) with its basic wavelength in excess of 240 km (the east–west dimension of the survey) and its ridge in the west and detached anticyclone in the northeast.

The modeled field of vertical velocity is related to the streamline pattern as expected from the theory of baroclinically unstable waves and meteorological experience (e.g., Holton 1979; Gill 1982); it is marked by rising motion at the downstream, and sinking motion at the upstream edge of troughs. This relation holds during the entire model run but is seen most easily while the meander structure remains a simple sinusoidal wave (compare top panels in Figs. 1 and 2). The regions of rising and sinking motion are clearly separated. During the quasi-sinusoidal meander phase there as many up- and downwelling regions as there are troughs and ridges.

After the meander amplitude has grown and the basic zonal wavenumber changed from $\kappa = 3$ to $\kappa = 1$, wavelike undulations occur along parts of the basic meander structure [e.g., along the northward flowing jet in the center of the model domain at day 50 (Fig. 1 middle) or along the left-hand edge of the broad trough at day 60 (Fig. 1 bottom)]. These secondary instabilities of about 40–50 km horizontal wavelength (measured along the basic meander), even if of small amplitude in the streamline pattern, are associated with intense vertical motions of the same horizontal scale (cf. Fig. 2 middle and bottom).

The extreme values of vertical motion increase continuously during the model run (Table 1), reaching downwelling and upwelling velocities of -72.9 and 40.7 m d^{-1}, respectively, at day 60. In parallel with an overall increase, the vertical velocity spectrum broadens with energy becoming distributed more uniformly (not shown); while the variance density (variance per wavelength) increases from day 20 to 50 by about one order of magnitude at the spectral peak at 85-km wavelength, it increases even more (by about two or even three orders of magnitude) at the largest (256 km) and smallest (4 km) resolved wavelengths.

The whitening in the vertical velocity spectrum is reproduced by all the three diagnostic methods tested, with no clear differences among them. Significant differences exist among them regarding their ability to diagnose the horizontal distribution of vertical velocity correctly.

The best diagnosis of the horizontal pattern of vertical motion is provided by the method using Q vectors.

FIG. 4. Coherence and phase spectra of the horizontal distributions of vertical motion at days 20 and 50 of the model run: modeled vertical velocity vs convergence of Q vectors.

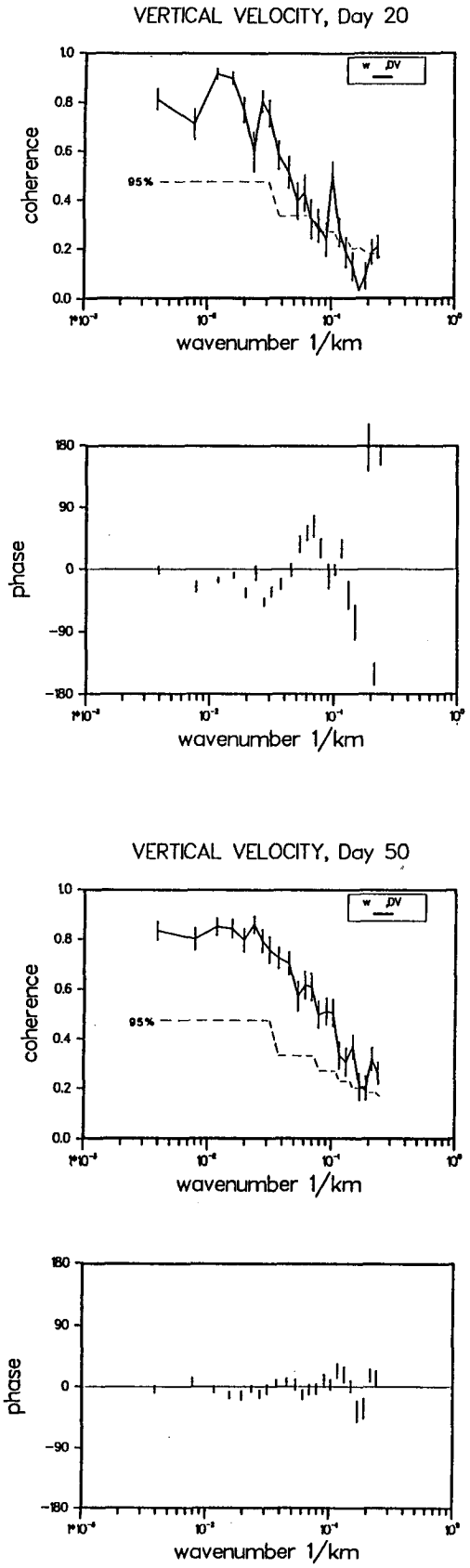

The convergence field of Q vectors closely resembles the modeled pattern of vertical velocity (cf. Fig. 3 top with Fig. 2 middle, showing, e.g., the patterns at day 50). Both fields are coherent, significantly correlated at the 95% confidence level for all scales, throughout the 60 days of integration (statistically analyzed at 10-day intervals, and illustrated with days 20 and 50 in Fig. 4). The phase varies in a narrow band around 0 deg. However, the coherence tends to decrease for the higher wavenumbers (horizontal wavelengths below about 10 km) where the vertical velocity variance increases strongest as integration time proceeds. The 95% confidence levels (in all the spectra shown) are estimated on the assumption that 13 out of the 128 data rows that are distributed over the meridional model extent of 256 km are statistically independent, with a number of 13 being suggested by the typical decorrelation scale of the most salient vertical motion spots of 20 km (half of their wavelength of about 40 km, e.g., Fig. 2).

Next in diagnostic accuracy is the method based on the advection of vorticity. The field of divergence implied by the advection of relative vorticity (cf. the example of day 50 in Fig. 3 middle with Fig. 2 middle) is coherent, significantly correlated with the modeled pattern of vertical velocity for the most scales throughout the time of the model run (Fig. 5). The drop of coherence toward the higher wavenumbers, however, begins already at larger wavelengths (at about 30 km) compared with the Q-vector method, and the phase, varying around 0 degrees, has a less tight relationship to the modeled vertical velocity.

The least reliable of the methods tested is that based on the isopycnic advection equation. Although the method is suitable for revealing the gross distribution of vertical motion (Fig. 3 bottom), it does not diagnose correctly the individual spots of upwelling and downwelling; in many instances upwelling is diagnosed where downwelling should occur, and downwelling is diagnosed where upwelling should occur (cf. Fig. 2 middle). This false diagnosis of the phase relationship is the most striking difference to the two other methods. Whereas the phase also varies around 0 deg but within a broader band, in the earlier quasi-sinusoidal stage of meander development it drifts off, ending at about 180 deg. This drift occurs continuously with integration time: at day 20, as shown in Fig. 6, the phase varies between −30 and 90 deg (a positive phase means the modeled vertical velocity field is leading), at days 30 and 40 it varies between 50 and 170 deg, at day 50 between 130 and 190 deg (Fig. 6), and at day 60 between 140 and 190 deg. The overall correlation is not

FIG. 5. Coherence and phase spectra of the horizontal distributions of vertical motion at days 20 and 50 of the model run: modeled vertical velocity vs divergence implied by vorticity advection.

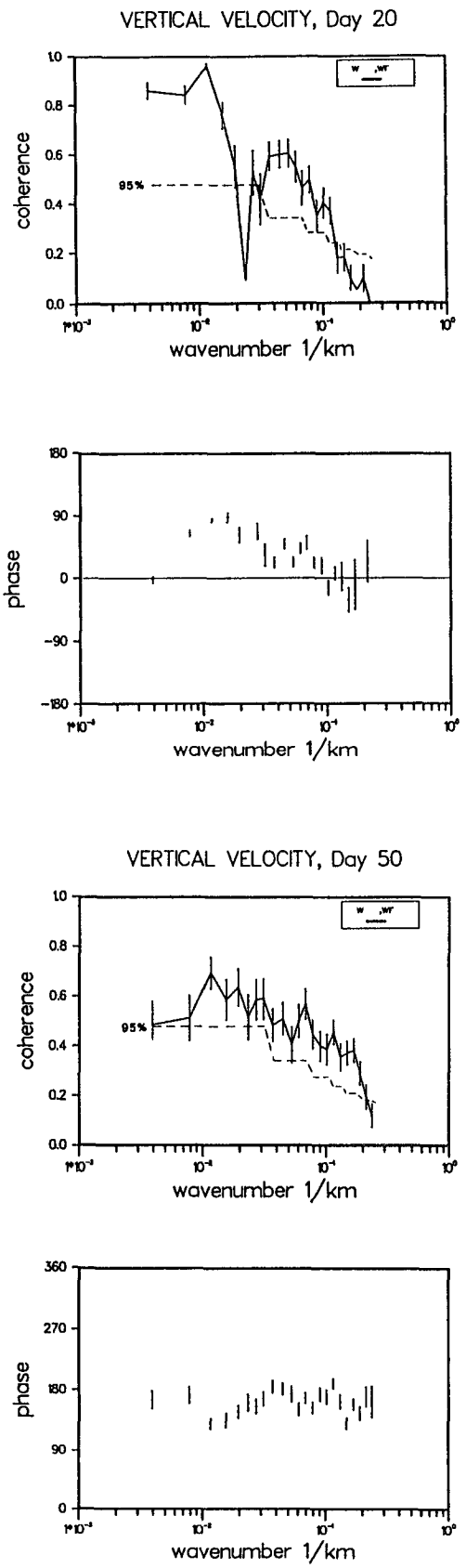

as high as with the two earlier methods (Fig. 6), but the diagnosed and modeled fields of vertical velocity are significantly coherent for many scales also in this case. Hence, the vertical velocity field diagnosed by use of the isopycnic advection equation is coherent with the modeled pattern, but upwelling is implied where downwelling should occur, and vice versa, when the streamlines are broken up in meanders and eddies and secondary instabilities have developed along the larger-scale meander structure.

For the first two diagnostic methods (vorticity advection and Q vectors), which imply a pattern of vertical motion coherent and of equal phase with the modeled vertical velocity distribution, it is worth also comparing the amplitudes of the diagnosed and modeled fields. Figure 7 shows the results of a linear regression of the modeled vertical velocity amplitude with the amplitudes of (a) the divergence diagnosed from the vorticity advection, (b) the convergence of Q vectors, and in addition (c) the Q-vector potential [defined with Eq. (13) in the companion paper by Fiekas et al.]. As a measure of amplitude, and its evolution in time, the absolute minima and maxima in the diagnosed and modeled distributions at days 20, 30, 40, 50, and 60 are taken (see also Table 1). In all three cases, the amplitudes of the diagnosed and modeled fields are significantly correlated at the 99% confidence level, assuming a linear relationship. To obtain a quantitative estimate of vertical motion (in units of m d^{-1}) from the divergence (in d^{-1}) implied by the vorticity advection, the divergence has to be multiplied by a factor of 39 m and a small offset of 4 m d^{-1} has to be subtracted. The convergence of Q vectors (in units of m^{-1} d^{-1}) can be converted into vertical motion by multiplication by a factor 26 m^2 and subtraction of 2 m d^{-1}. The Q-vector potential gives an estimate of vertical motion already in the right units; only a small correction factor of 0.8 and an offset addition of 0.5 m d^{-1} has to be applied.

4. Discussion

The modeled spots of vigorous vertical motion, exceeding 10 m d^{-1}, occur at horizontal wavelengths of a few tens of kilometers. This corresponds to the scale of mesoscale upwelling indicated by the typical size of observed chlorophyll patches (Strass 1992).

In the model, the vertical velocity tends to be higher when it occurs at smaller horizontal scales. This tendency is also revealed by observations: Leach (1987) diagnosed vertical velocities of 0.6 m d^{-1} distributed wavelike along a meander structure 100 km wide, Fie-

FIG. 6. Coherence and phase spectra of the horizontal distributions of vertical motion at days 20 and 50 of the model run: modeled vertical velocity vs vertical velocity resulting from isopycnic advection.

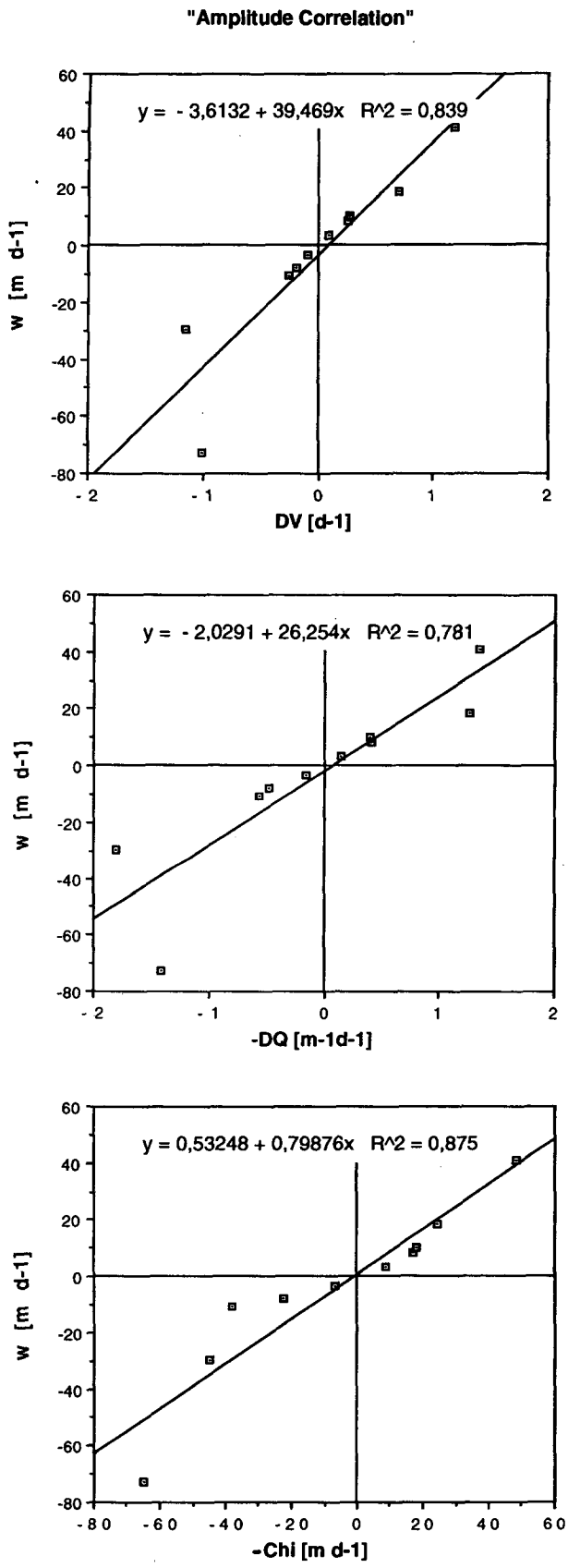

kas et al. obtained 5 m d^{-1} at a horizontal wavelength of 85 km, and Pollard and Regier (1992) derived vertical motions of up to 40 m d^{-1} at horizontal wavelengths of 40–80 km. The 5 m d^{-1} of Fiekas et al. compare well with the 3 or 8 m d^{-1} in the modeled pattern at day 20 or 30 when the horizontal scales were dominated by a wavelength of also 85 km; that is, the vertical velocity amplitudes either obtained from measurements or modeled are similar if related to the appropriate horizontal scales.

In the model as well as in the data analysis of Fiekas et al. the most intense vertical motions were associated with secondary instabilities growing on the basic meander structure. However, the horizontal scales of vertical motion in the model and in the observations may differ. In the observations, representing one instantaneous (quasi-synoptic) snapshot, the basic meander has a wavelength in excess of 240 km (the east–west dimension of the survey) and the secondary instabilities occur at a wavelength of 85 km. In the model, the wavelength of the secondary instabilities changes during integration time. At day 20 of the model run they are of also 85 km wavelength. At day 60, when a large-scale meander structure of 256-km wavelength has developed, the secondary instabilities are distributed along it at a wavelength of 40–50 km.

Testing Q vectors, vorticity advection, and isopycnic advection as diagnostic methods for vertical motion has shown that the horizontal distributions of the convergence of Q vectors as well as of the divergence implied by vorticity advection are coherent with the mesoscale pattern of vertical velocity, and these two fields also obey the correct phase relationships; but higher correlation extending further toward smaller scales and a closer phase relation indicates that the Q-vector method is superior.

By application of the isopycnic advection equation, however, a vertical motion field may be obtained that is inversely correlated to the real one. Most obviously, the inverse relationship results from neglecting the tendency term in the adiabatic thermodynamic equation when deriving the isopycnic advection [Eq. (8) in Fiekas et al.]. Together with treating isopycnic surfaces as material surfaces where a kinematic boundary condition applies, the stationarity assumption becomes fatal when the ageostrophic velocity gains relative importance.

FIG. 7. Correlation of the amplitude of the modeled vertical velocity, w, with the amplitudes of vertical motion implied by the divergence diagnosed from the vorticity advection (denoted DV, top), the convergence of Q vectors (denoted −DQ, middle), and the Q-vector potential (denoted Chi, bottom). The amplitudes (minima and maxima) are extracted from days 20, 30, 40, 50, and 60 of the model run, resulting in 10 data points (printed in Table 1) for each regression. The regression coefficients, assuming a linear relationship, are given in each diagram together with the squared correlation coefficients, R^2.

Consider the case where the ageostrophic flow is from the lighter to the denser water, that is, where the current vector is directed to isopycnic surfaces sloping upward in the direction of the flow. Stationarity then would suggest upward motion because the water has to ascend along the isopycnic surfaces. In the nonstationary case, on the other hand, dense water would be substituted by the advection of light water, and isopycnic surfaces would be shifted downward, indicating downwelling.

Scaling factors needed to convert either the divergence implied by vorticity advection, the convergence of Q vectors, or the Q-vector potential into vertical velocity have been obtained by linear regression of the respective amplitudes. The scaling factors used by Fiekas et al. in their data analysis do not deviate much from those obtained. For scaling the vorticity divergence the amplitude regression yielded a factor of 39 m; Fiekas et al., and earlier Leach (1987), used a depth scale of 50 m. For the convergence of Q vectors no scaling has been used in the companion paper or in Leach (1987), but instead the Q-vector potential was introduced to obtain an estimate of vertical velocity from the Q-vector field. According to the amplitude regression, only a small correction factor of 0.8 has to be applied to the Q-vector potential. However, the Q-vector potential is somewhat smoothed compared to the Q-vector field itself.

5. Conclusions

Patterns of vertical motion diagnosed from combined density and horizontal velocity mappings by application of the Q-vector version of the ω equation are likely to resemble nature qualitatively. Moreover, in the quantitative sense, it seems possible using an appropriate scaling to also obtain the amplitude of vertical velocity correctly to an error of a few tens of percent.

Acknowledgments. The author is indebted to Dr. H. Leach for encouragement of this study and for his comments on the manuscript, and to Dr. R. Onken for making available the model code. The model calculations were carried out during the author's previous position at the Institut für Meereskunde an der Universität Kiel, Germany. The work has been financially supported by the Deutsche Forschungsgemeinschaft through "Teilprojekt B1," which formed part of the "Sonderforschungsbereich 133, Warmwassersphäre des Atlantik."

REFERENCES

Bleck, R., 1979: Finite-difference equations in generalized vertical coordinates. Part II: Potential vorticity conservation. *Contrib. Atmos. Phys.*, **52,** 95–105.

——, and D. B. Boudra, 1981: Initial testing of a numerical ocean circulation model using a hybrid (quasi-isopycnic) vertical coordinate. *J. Phys. Oceanogr.*, **11,** 755–770.

——, and L. T. Smith, 1990: A wind-driven isopycnic coordinate model of the northern equatorial Atlantic Ocean. 1. Model development and supporting experiments. *J. Geophys. Res.*, **95,** 3273–3286.

——, H. P. Hansen, D. Hu, and E. B. Kraus, 1989: Mixed layer–thermocline interaction in a three-dimensional isopycnic coordinate model. *J. Phys. Oceanogr.*, **19,** 1417–1439.

Boudra, B. D., R. Bleck, and F. Schott, 1988: A numerical model of instabilities in the Florida Current. *J. Mar. Res.*, **46,** 715–751.

Fiekas, V., H. Leach, K.-J. Mirbach, and J. D. Woods, 1994: Mesoscale instability and upwelling. Part 1: Observations at the North Atlantic intergyre front. *J. Phys. Oceanogr.*, **24,** 1750–1758.

Gill, A. E., 1982: *Atmosphere–Ocean Dynamics.* Academic Press, 662 pp.

Holton, J. R., 1979: *An Introduction to Dynamic Meteorology,* 2d ed. Academic Press, 391 pp.

Hoskins, B. J., and M. A. Pedder, 1980: The diagnosis of middle latitude synoptic development. *Quart. J. Roy. Meteor. Soc.*, **106,** 707–719.

——, I. Draghici, and H. C. Davis, 1978: A new look at the ω-equation. *Quart. J. Roy. Meteor. Soc.*, **104,** 31–38.

Leach, H., 1987: The diagnosis of synoptic-scale vertical motion in the seasonal thermocline. *Deep-Sea Res.*, **34**(12A), 2005–2017.

Onken, R., 1986: Numerische Simulation der Erzeugung und Instabilität mesoskaliger Fronten. *Ber. Inst. Meereskd. Univ. Kiel,* **156,** 188 pp.

——, 1992: Mesoscale upwelling and density finestructure in the seasonal thermocline—A dynamical model. *J. Phys. Oceanogr.*, **22,** 1257–1273.

——, and B. Klein, 1991: A model of baroclinic instability and waves between the ventilated gyre and the shadow zone of the North Atlantic Ocean. *J. Phys. Oceanogr.*, **21,** 53–67.

Pedlosky, J., 1987: *Geophysical Fluid Dynamics,* 2d ed. Springer-Verlag, 710 pp.

Pollard, R. T., and L. A. Regier, 1992: Vorticity and vertical circulation at an ocean front. *J. Phys. Oceanogr.*, **22,** 609–625.

Strass, V. H., 1992: Chlorophyll patchiness caused by mesoscale upwelling at fronts. *Deep-Sea Res.*, **39**(1A), 75–96.

Tintoré, J., D. Gomis, S. Alonso, and G. Parrilla, 1991: Mesoscale dynamics and vertical motion in the Alboran Sea. *J. Phys. Oceanogr.*, **21,** 811–823.

Woods, J. D., 1988: Mesoscale upwelling and primary production. *Towards a Theory of Biological–Physical Interactions in the World Ocean,* B. J. Rothchild, Ed., Kluwer Academic, 7–38.